ACS APPLIED MATERIALS & INTERFACES

Research Article

www.acsami.org

Enhanced Adsorptive Removal of Methyl Orange and Methylene Blue from Aqueous Solution by Alkali-Activated Multiwalled Carbon Nanotubes

Jie Ma,[†] Fei Yu,*[,†,‡] Lu Zhou,[†] Lu Jin,[†] Mingxuan Yang,[†] Jingshuai Luan,[†] Yuhang Tang,[†] Haibo Fan,[†] Zhiwen Yuan,[†] and Junhong Chen*[,†,§]

[†]State Key Laboratory of Pollution Control and Resource Reuse, School of Environmental Science and Engineering, Tongji University, 1239 Siping Road, Shanghai 200092, China

[‡]School of Environmental Science and Engineering, Shanghai Jiao Tong University, 800 Dong Chuan Road, Shanghai 200240, China.

[§]Department of Mechanical Engineering, University of Wisconsin−Milwaukee, Milwaukee, Wisconsin 53211

Supporting Information

ABSTRACT: An alkali-acitvated method was explored to synthesize activated carbon nanotubes (CNTs-A) with a high specific surface area (SSA), and a large number of mesopores. The resulting CNTs-A were used as an adsorbent material for removal of anionic and cationic dyes in aqueous solutions. Experimental results indicated that CNTs-A have excellent adsorption capacity for methyl orange (149 mg/g) and methylene blue (399 mg/g). Alkali-activation treatment of CNTs increased the SSA and pore volume (PV), and introduced oxygen-containing functional groups on the surface of CNTs-A, which would be beneficial to improving the adsorption affinity of CNTs-A for removal of dyes. Kinetic regression results shown that the adsorption kinetic was more accurately represented by a pseudo second-order model. The overall adsorption process was jointly controlled by external mass transfer and intra-particle diffusion, and intra-particle diffusion played a dominant role. Freundlich isotherm model showed a better fit with adsorption data than Langmuir isotherm model. Adsorption interactions of dyes onto CNTs-A from aqueous solutions were investigated using Fourier transform infrared (FT-IR) spectroscopy, scanning electron microscopy (SEM), X-ray diffraction (XRD), and Brunauer−Emmett−Teller (BET) method. The remarkable adsorption capacity of dye onto CNTs-A can be attributed to the multiple adsorption interaction mechanisms (hydrogen bonding, $\pi-\pi$ electron−donor−acceptor interactions, electrostatic interactions, mesopore filling) on the CNTs-A. Results of this work are of great significance for environmental applications of activated CNTs as a promising adsorbent nanomaterial for organic pollutants from aqueous solutions.

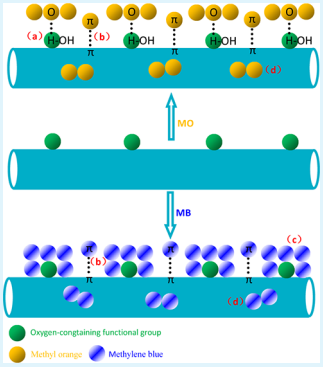

KEYWORDS: *dye, adsorption, multiwalled carbon nanotubes, alkali activation,*

1. INTRODUCTION

Color wastewater has been produced ever since the dye technique was invented, with various synthetic dyes used in a wide range of industries such as textile, leather, paper, printing, and other industries.[1] It is rather difficult to treat dye wastewater because their synthetic origins and mainly aromatic structure are biologically non-degradable. Among many chemical, physical, and biological treatment methods, adsorption technology is one of the most effective methods for dye removal because of its low cost, high efficiency, simplicity, and insensitivity to toxic substances.[2−5] Methyl orange (MO) and methylene blue (MB) are well-known anionic and cationic dyes, which have been widely used in textile, printing, and research laboratories. Hence, MO and MB were selected as representative target pollutants in this study.

High-capacity adsorbent for removal of dyes from solution is still under development to reduce the adsorbent price and to resolve disposal problems. Multi-walled carbon nanotubes (CNTs) have been attracting increasing research interest recently because of their novel properties like high aspect ratio and excellent thermal, electrical, and mechanical properties.[6] Structurally, their large specific surface areas, hollow and layered structures make them an ideal adsorption material.[7] More importantly, the excellent adsorption ability of CNTs relative to other adsorbents may be due to strong interactions between CNTs and target compounds through $\pi-\pi$ electron coupling,[8,9] which result from the delocalized electrons in hexagonal arrays of carbon atoms on the surface of CNTs. As adsorbent materials, CNTs are required to possess a high SSA and PV, which could provide enough adsorption sites for hazardous pollutants in wastewater treatment and make them a possible candidate for water purification.[10] Nevertheless, compared with activated carbon, most CNTs currently reported in the literature generally have a relatively lower

Received: June 13, 2012
Accepted: October 12, 2012
Published: October 12, 2012

SSA in the range of 100-300 m^2/g. Therefore, activated carbon is still the dominant adsorbent widely used for removal of dyes from the aqueous solution.[11−13] However, activated carbon also presents significant disadvantages. It is flammable and difficult to regenerate. In addition, activated carbon have weak hydrophilic properties, resulting in the weak affinity for the adsorption of cationic or anionic dyes from aqueous solutions.[14]

CNTs are currently produced in large quantities at a low cost. Therefore, CNTs are more likely to find affordable appliacations as commercial sorbents. However, CNTs' relatively lower SSA than activated carbon has hindered their potential applications as promising adsorbents for organic contaminants. Moreover, unlike the fixed pore structure of activated carbon, the mesoporous interstices and grooves formed by nano-aggregation of CNTs are flexible and thus susceptible to structural alterations induced by strong adsorptive interactions. To improve the adsorption properties of CNTs, researchers have applied various synthesis techniques and post-treatment approaches. Among these methods, modification via alkali-activation appears to be an effective route to improve the SSA and PV.[15,16] For instance, activated CNTs have been perspective candidates for hydrogen adsorption storage[17] and supercapacitors.[18] Similarly, it is reasonable to hypothesize that activated CNTs would be superb adsorbents for dyes; however, no relevant studies have been performed thus far.

In this paper, we report on an alkali-activation method to synthesisize activated CNTs (CNTs-A) with higher SSA and PV through producing large quantities of meso-PV. And then CNTs-A was first used as an adsorbent material for removal of anionic and cationic dyes in aqueous solutions. Excellent adsorption properties have been realized for anionic dye (MO) and cationic dye (MB) on CNTs-A. Comparisons of adsorption properties for one type of dye on CNTs before and after activated treatment and two different dyes on one adsorbent were further investigated. These results indicate that alkali-activation is a useful method to improve the adsorption affinity of dye contaminants on CNTs. Therefore, CNTs-A may be a promising adsorbent nanomaterial for organic pollutants from aqueous solutions.

2. MATERIALS AND METHODS

2.1. Material and Chemicals. All chemicals were purchased from Sinopharm Chemical Reagent Co., Ltd (Shanghai, China) in analytical purity and used in the experiments directly without any further purification. All solutions were prepared using deionized water. The main characteristics and structures of MO and MB are shown in Table S1 in the Supporting Information. The present CNTs were prepared by the catalytic chemical vapor deposition method[19] and purified using a nondestructive approach.[20] CNT sample contained >95% carbon nanotubes, with the outer diameter of CNTs ranging from 20 to 30 nm and the number of walls in CNTs ranging from 10 to 20. A mixture of purified CNTs and KOH powder was performed in a stainless steel vessel in an inert gas atmosphere. The weight ratio of KOH to CNTs was 6:1. The mixing time was 10 min to obtain a uniform powder mixture. The mixture was then heated to 1023 K for 1 h under flowing argon in a horizontal tube furnace, washed in concentrated hydrochloric acid and the deionized water, and then dried.

2.2. Batch Adsorption Experiments. Dye concentration was determined colorimeterically by measuring at maximum absorbance of the two dyes (λ_{max} = 463 nm for MO and λ_{max} = 631 nm for MB). A calibration curve was plotted between absorbance and concentration of the dye to obtain the absorbance-concentration profile of the dye based on Beer-Lambert's law. For high concentration dyes, dye samples were diluted before absorbance measurements. The concentration of the dye in the solution was determined by the Beer-Lambert's law expression.[21] Batch adsorption experiments were conducted in 50 ml glass bottles with 30 mg CNTs or CNTs-A and 40 mL of dye solution of different initial concentrations of 80−150 mg/L for MO and 200−270 mg/L for MB, and the pH of the solution was adjusted to ∼7.0 (nearly in neutral solution to avoid the unpredictable influence) with HCl or NaOH solutions. Timing of the sorption period started as soon as the solution was poured into the bottle. Sample bottles were shaken on a shaker (TS-2102C, Shanghai Tensuclab Instruments Manufacturing Co., Ltd., China) and operated at a constant temperature of 25 °C and 150 rpm for 3 h. Preliminary experiments indicated that the adsorption of MO or MB reached equilibrium in ∼1.5 h. Thus, the contact time of 3 h was selected in the batch experiments. All adsorption experiments were conducted in duplicate, and only the mean values were reported. The maximum deviation for the duplicates was usually less than 5%. The blank experiments without the addition of CNTs or CNTs-A were conducted to ensure that the decrease in the concentration was actually due to the adsorption of CNTs or CNTs-A, rather than by the adsorption on glass bottle wall. After adsorption equilibrium has been achieved, the MO or MB concentrations of the solutions were measured using a spectrophotometer (UV759UV-VIS, Shanghai Precision &Scientific Instrument Co. Ltd.). Kinetic studies were performed at a constant temperature of 25 °C and 150 rpm with 150(MO) and 500(MB) mg/L initial concentration of dye solutions. The ionic strength experiments were conducted in 150 mg/L MO and 350 mg/L MB solution also at pH 7, with varying concentrations (0.05, 0.1, 0.2, 0.4 mol/L) of NaCl solution. The effect of solution pH on dye removal was studied in the range of 2−10 with 150 mg/L (MO) and 500 mg/L (MB) initial concentrations of dye solutions. The initial pH values of all the solutions were adjusted using 0.1 mol L^{-1} HCl or 0.1 mol L^{-1} NaOH solution with desired concentrations.

The amount of adsorbed dye on adsorbents (q_t, mg/g) was calculated as follows

$$q_t = (C_0 - C_t)\frac{V}{m} \quad (1)$$

where c_0 and c_t are the dye concentrations at the beginning and after a period of time (mg/L), V is the initial solution volume (L); and m is the adsorbent weight (g).

2.3. Characterization Methods. The microstructure and morphology of the CNTs, CNTs-A, and MO/MB adsorbed CNTs-A were analyzed by high-resolution transmission electron microscopy (HRTEM, JEOL 2100F, Japan) and scanning electron microscopy-(SEM,JSM-6400F). X-ray diffraction (XRD) experiments were conducted on specimens using a X-ray diffractometer (Bruker D8 Advance, Bruker AXS, Germany) operating at 40 KV and 40 mA. Nickel-filtered Cu $_{Ka}$ radiation was used in the incident beam. The SSA and pore size distribution of adsorbents were calculated from the adsorption/desorption isotherms of N_2 at 77K by multi-point BET and Barrett-Joyner-Halenda (BJH) method using a BELSORP instrument (BEL, Japan, Inc.). X-ray photoelectron spectroscopy (XPS) analysis was carried out in a Kratos Axis Ultra DLD spectrometer, using monochromated Al Ka X-rays, at a base pressure of 1×10^{-9} Torr. Survey scans determined between 1100 and 0 eV revealed the overall elemental compositions of the sample and regional scans for specific elements were performed. The peak energies were calibrated by placing the major C_{1s} peak at 284.6 eV. Samples were prepared identically to those of the batch experiments. Fourier transform infrared (FTIR) spectra of powder samples were recorded on a Tensor 27 FTIR spectrometer (Bruker Optics, Inc.). The zeta potential of adsorbents were measured by Zetasizer apparatus (Nano Z, Malvern Instruments Ltd., UK.). The procedure used to calculate the pHzpc (zero point of charge) of all samples was potentiometric titration based on the acid-base reaction,[22,23] 0.1 M HCl and NaOH aqueous solutions were used during the potentiometric tritation. TA Instruments Q600 SDT thermal analyzer was used for high resolution thermogravimetric analysis (TGA) and differential thermal analysis

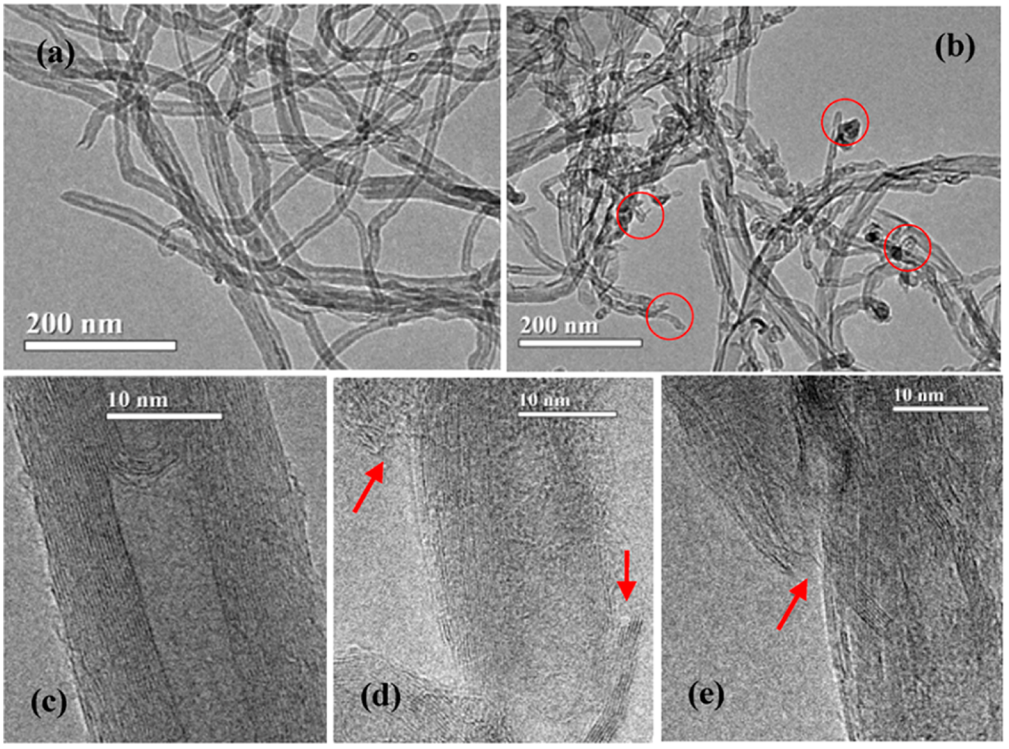

Figure 1. HRTEM images of (a, c) CNTs and (b, d, e) CNTs-A.

(DTA). TGA and DTA curves were obtained by heating approximately 10 mg of finely samples from 50 to 900 °C at a heating rate of 10 °C/min in air.

2.4. Data Analysis. *2.4.1. Isotherm Model. Langmuir Model.* The form of the Langmuir isotherm can be represented by the following equation:

$$q_e = q_m \frac{K_L C}{1 + K_L C} \tag{2}$$

where q_e is the amount of dye adsorbed per gram of adsorbent (mg/g), C denotes the equilibrium concentration of dye in solution (mg/L); K_L represents the Langmuir constant (L/mg) that relates to the affinity of binding sites, and q_m is a theoretical limit of adsorption capacity when the monolayer surface is fully covered with dye molecules to assist in the comparison of adsorption performance (mg/g). Furthermore, the effect of the isotherm shape was studied to understantwhether an adsorption system is favorable or not. Another important parameter, R_L, called the separation factor or equilibrium parameter, which can be used to determine the feasibility of adsorption in a given concentration range over adsorbent, was also evaluated from the relation[24]

$$R_L = \frac{1}{1 + K_L C_0} \tag{3}$$

where K_L is the Langmuir adsorption constant (l/mg) and C_0 is the initial dye concentration (20 mg/L). Ho and McKay[25] established that (1) $0 < R_L < 1$ for favorable adsorption; (2) $R_L > 1$ for unfavorable adsorption; (3) $R_L = 1$ for linear adsorption; and (4) $R_L = 0$ for irreversible adsorption.

Freundlich Model. The Freundlich isotherm model has the following form

$$q_e = K_F C^{1/n} \tag{4}$$

where q_e is the amount of dye adsorbed per gram of adsorbent (mg/g); C is the equilibrium dye concentration in solution (mg/L); K_F and n are the Freundlich constants, which represent the adsorption capacity and the adsorption strength, respectively. The magnitude of $1/n$ quantifies the favorability of adsorption and the degree of heterogeneity of the adsorbent surface.

Dubinin–Radushkevich (D-R) Model. The D-R isotherm model has the following form:

$$\ln q_e = \ln q_m - B\varepsilon^2 \tag{5}$$

where B is a constant related to the mean free energy of adsorption (mol^2/kJ^2), q_m is the theoretical saturation capacity, and ε is the Polanyi potential, which is equal to

$$\varepsilon = RT\ln\left(1 + \frac{1}{C}\right) \tag{6}$$

where R (J mol^{-1} K^{-1}) is the gas constant and T (K) is the absolute temperature. For D-R isotherm model, from B values the mean energy of adsorption. E can be calculated using the relation[26]

$$E = \frac{1}{\sqrt{-2B}} \tag{7}$$

On the basis of eqs 5, 6, and 7, the isotherm constants, E and determination coefficients were calculated. The mean energy of adsorption (E) is the free energy change when one mole of the ion is transferred from infinity in the solution to the surface of the solid.

2.4.2. Kinetic Model. Pseudo-First- and Pseudo-Second-Order Model. The linear form of pseudo-first-order rate equation is

$$\ln(q_e - q_t) = \ln q_e - \frac{K_1}{2.303} t \tag{8}$$

where q_e and q_t are the amounts of MO adsorbed (mg/g) at equilibrium and time t (min), respectively; K_1 is the rate constant of the pseudo first-order kinetic model (min^{-1}).[25]

A linear form of pseudo second-order kinetic model is express by eq 9

$$\frac{t}{q} = \frac{1}{k_2 q_e^2} + \frac{t}{q_e} \tag{9}$$

where k_2 is the rate constant(g mg^{-1} min^{-1}) of pseudo second-order kinetic model for adsorption.[25]

dx.doi.org/10.1021/am301053m | ACS Appl. Mater. Interfaces 2012, 4, 5749–5760

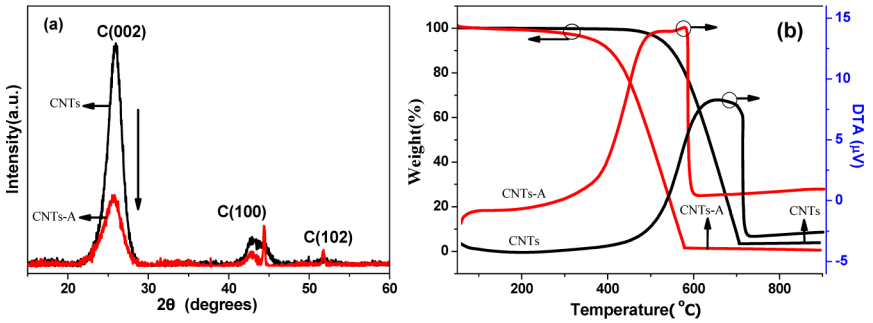

Figure 2. (a) XRD data and (b) thermal analysis curve of the CNTs and CNTs-A.

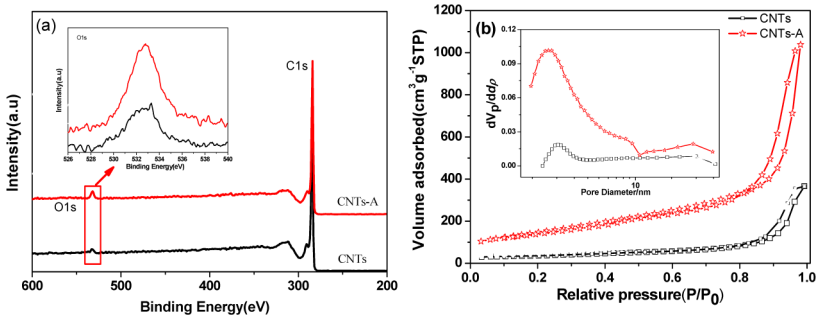

Figure 3. (a) XPS survey scans and O1s deconvolution and (b) N_2 adsorption/desorption isotherms and pore size distribution of CNTs and CNTs-A.

Weber–Morris Kinetics Model. Intra-particle mass transfer diffusion model proposed by Weber and Morris can be written as follows[27]

$$q_t = k_i t^{1/2} + C \tag{10}$$

where C (mg/g) is the intercept and k_i is the intra-particle diffusion rate constant (g mg^{-1} min$^{-0.5}$) for adsorption.

Boyd Model. Boyd model[28] has the following form

$$Bt = -\ln\left(1 - \frac{q_t}{q_e}\right) - 0.4977 \tag{11}$$

where q_t and q_e are the amounts of dyes adsorbed on the adsorbent (mg g^{-1}) at time t (min) and at equilibrium time (minute), respectively; $B = \pi^2 D_i/r^2$ (D_i is the effective diffusion coefficient of the adsorbate and r is the radius of adsorbent particles assumed to be spherical).

3. RESULTS AND DISCUSSION

3.1. Characterization of the Adsorbent. Figure 1a displays the HRTEM image of CNTs. It can be seen that CNT diameter is 20−30 nm and the CNT length is several hundred nanometers to one micrometer. The crystal structure was studied by XRD, which indicate a well graphite nature (Figure 2a). The HRTEM of CNTs (Figure 1c) shows the CNTs have a good tubular structure and smooth shell with few defects. However, after activated treatment, the CNT experienced an obvious structural change. CNTs-A's length is obviously shortened to about 300−500 nm compared with CNTs. Furthermore, part of the hollow tubular structure is destroyed, and a large number of defects are produced (the arrow in Figure 1). The tips of tube are mainly opened (the circle in Figure 1), and many flaky apertures are generated on the surface. Peaks of C with relatively high intensity and symmetry are clearly observed in Figure 2a. This observation suggests that the graphite structure remained even after strong activation reactions.

In Figure 2b, the TGA curves of CNTs and CNTs-A exhibit two main weight loss regions. CNTs are considerably stable and show a little weight loss close to 5% below 200 °C in the first region, which can be attributed to the evaporation of adsorbed water and the elimination of oxygen-containing functional groups on the surface of CNTs. The rapid weight loss region can be attributed to the decomposition of carbon in the CNTs. Comparing CNTs with CNTs-A, it is clearly seen that the main thermal events temperature (T_m) decreased from ∼650 to ∼530 °C, as shown in Figure 2b, which may be attributed to the CNTs structure defects and more oxygen-containing functional groups produced by activated treatment, but the T_m is so high that CNTs-A could meet the application needs of adsorbent in water treatment. The composition of CNTs and CNTs-A was determined by XPS as shown in Figure3a. The asymmetric nature and intensity of the C_{1s} peak remain almost unchanged after activated treatment. The observed asymmetric tailing is a result of the presence of some surface functionality of both kinds of CNTs. The CNTs show a small O_{1s} signal with an atomic content of 1.63 %, in comparison with 3.31 % for CNTs-A. This observation reveals minimal introduction of new oxygen-containing functional groups on the surface of CNTs.

The N_2 adsorption/desorption isotherms of CNTs and CNTs-A are presented in Figure 3b. In comparison, the N_2 adsorption/desorption amount of CNTs-A is considerably higher than that of CNTs at low or high pressure. The detailed features of meso-pore analyzed by the BJH method are presented in Table 1. The SSA and PV of CNTs-A drastically increased by about ∼4.3 and ∼2.8 times than CNTs, respectively. Such increases correspond to a decrease in mean pore diameter from ∼18.3 to ∼12 nm. Moreover, the meso-SSA and meso-PV of CNTs-A are improved by ∼6.3 and ∼2.8 times compared to that of CNTs. Despites the decrease in micro-SSA and micro-PV, the considerable amount of meso-

Table 1. Physical Properties of CNTs, CNTs-A, and MO/MB Adsorbed CNTs-A[a]

adsorbents	SSA	ISA	ESA	APD	PV	O%	SSA/O%
CNTs	123.5	38.9	84.5	18.3	0.59	1.63	75.8
CNTs-A	534.6	0	534.6	12	1.61	3.31	161.5
CNTs-A-MO	582.5	0	582.5	8.6	1.50		
CNTs-A-MB	729.3	0	729.3	7.9	1.71		

[a]SSA= specific surface area (m^2/g); ISA = internal surface area (m^2/g); ESA = external surface area (m^2/g); PV = pore volume (cm^3/g); APD = average pore diameter (nm); O%: surface oxide (at. %) by XPS; SSA/O% means specific surface area normalized surface oxides values.

pore obviously takes a dominant role (Table 1). The mesopore distribution of the CNTs-A is similar to that of the pristine CNTs in the region of tens of nanometers. The stronger peak is located at d_p = 2.5 nm approximately. The difference lies in the abrupt increase in the volume distribution (d_{Vp}/d_p) of CNTs-A, especially near the micropore region, whereas the volume distribution of CNTs remains within a very low level. This indicates the presence of plenty of mesopores after alkali-activation treatment.

The above-mentioned results indicated that alkali-activation is a high-efficiency technique for producing a large scale of porous structures. The activation mechanism is normally suggested to include independent hydroxide and redox processes during the reaction. With the activation treatment, KOH powder can react with carbon as follows[29,30]

$$6KOH + C \rightarrow 2K + 3H_2 + 2K_2CO_3 \quad (12)$$

When the temperature is higher than 700 °C, the reaction proceeds as follows

$$K_2CO_3 + C \leftrightarrow K_2O + 2CO \quad (13)$$

$$K_2CO_3 \leftrightarrow K_2O + CO_2 \quad (14)$$

$$2K + CO_2 \leftrightarrow K_2O + CO \quad (15)$$

When the temperature is higher than 800 °C, the reaction proceeds as follows

$$K_2O + C \leftrightarrow 2K + CO \quad (16)$$

The entanglement of long CNTs also will reduce the useful surface area. After alkali-activated treatment, the entangled CNTs can be shortened and the dispersion is strongly improved. Most importantly, some of the graphitic structure will be destroyed. Not only the tube tip are opened, but also large quantities of new micro-pores and meso-pores even with open apertures are produced. This implies that the CNTs after the present activation treatment possess more micropores and mesopores, and could give rise to an obvious improvement in total SSA.

3.2. Adsorption Isotherms. Figure 4 shows the equilibrium isotherms for adsorption of dyes onto CNTs and CNTs-A, and the equilibrium adsorption characteristics were analyzed by using the Langmuir[31] and Freundlich[32] isotherm models. The isotherms based on the experimental data and the parameters obtained from nonlinear regression by both models are shown in Figure 4. Table 2 summarizes the determination coefficients (R^2) of the Langmuir and Freundlich isotherms of CNTs and CNTs-A. Based on the determination coefficient shown in Table 2, Freundlich isotherm model showed a better fit with adsorption data than Langmuir isotherm model. The applicability of Freundlich isotherm suggests that different sites with several adsorption energies are involved, and in some cases, the intermolecular interactions occur between dyes and CNTs.

Figure S1 in the Supporting Information shows that the computed maximum monolayer capacities are 46 mg/g for MO and 118 mg/g for MB on CNTs, and 149 mg/g for MO and 400 mg/g for MB on CNTs-A. Comparing adsorption properties of CNTs with CNTs-A adsorbents, two marked results should be mentioned: First, the adsorption capacity of MO or MB increased obviously almost by ~3.2 times for MO and ~3.4 times for MB after alkali-activated treatment; second, the adsorption capacity of MB dye is larger than the MO dye on CNTs or CNTs-A. As we know that only part of the total SSA is accessible for molecules to be adsorbed. Hence, adsorbents with a higher meso-porosity area are desirable. For CNTs-A, the micro-SSA and micro-PV decrease after the activated treatment, and meso-SSA and meso-PV are improved almost by ~6.3 and ~2.8 times. The considerable amount of meso-pore obviously takes a dominant role (as shown in Table 1). The molecule size of MO and MB is about ~2 nm (as shown in Table S1 in the Supporting Information), which is smaller than the average pore size (~12 nm). So meso-SSA and meso-PV would provide more adsorption sites for MO and MB. Hence, the above results might be caused by the significant differences of SSA and PV between CNTs (123.5 m^2/g and 0.587 cm^3/g) and CNTs-A (534.6 m^2/g and 1.61 cm^3/g). From the composition analysis of adsorbents, the oxygen atomic content of CNTS increased from 1.63 to 3.31 % after the activated treatment (as shown in Figure 3a). This result indicates that the surface of CNTs-A was modified by more oxygen-containing functional groups. Here, the surface oxygen content may affect the dispersibility of CNTs-A and the water

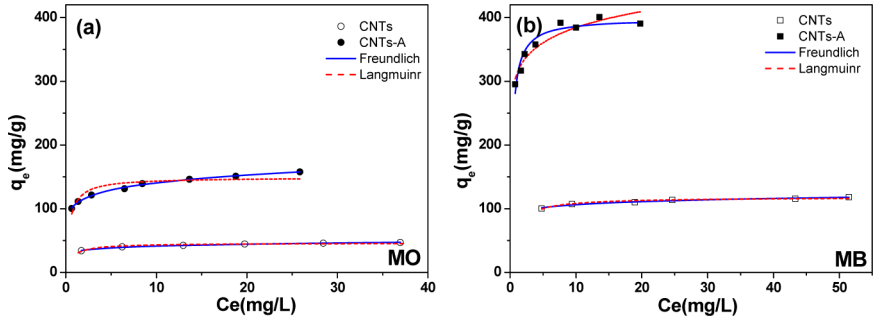

Figure 4. Equilibrium adsorption isotherms of (a) MO and (b) MB on CNTs and CNTs-A.

dx.doi.org/10.1021/am301053m | ACS Appl. Mater. Interfaces 2012, 4, 5749−5760

Table 2. Langmuir, Freundlich, and Dubinin−Radushkevich Isotherm Parameters of CNTs and CNTs-A

		Langmuir model			Freundlich model				Dubinin-Radushkevich model			
adsorbent	adsorbate	KL (l/mg)	q_m (mg/g)	R_L	R^2	K_F	$1/n$	R^2	B (mol/kJ^2)	Q_m (mg/g)	E (kJ/mol)	R^2
CNTs	MO	1.47	46	0.03	0.908	32.5	0.1	0.988	0.2	44.3	1.58	0.8427
CNTs-A	MO	2.45	149	0.02	0.837	106.4	0.12	0.996	0.06	130.7	2.88	0.8445
CNTs	MB	1.12	117.9	0.04	0.926	91.81	0.06	0.958	0.5	112.2	1	0.9281
CNTs-A	MB	3.05	399	0.016	0.911	310.8	0.09	0.900	0.06	376.2	2.88	0.9041

cluster formation in aqueous solution, which consequently can be favorable for the aqueous phase adsorption. With the increasing of oxygen content, maximum adsorption capacity is significantly enhanced. Similar results have been reported for toluene, ethylbenzene and xylene (TEX) adsorption on CNTs-NaClO.[33] Because MO and MB have good solubility, the main purpose of the surface functionalization of CNTs is to improve their hydrophilicity and dispersibility in aqueous solutions. A better dispersion of the CNTs-A in water will increase the available adsorption sites, which may be favorable for the aqueous phase adsorption. MO and MB have the same molecules size as shown in Table S1 in the Supporting Information, the q_m of MB is much greater than that of MO, which can be attributed to the more adsorption of cationic dye molecules on the negatively-charged surface of CNTs via a specific interaction like electrostatic interaction and ion exchange.[34]

The adsorption capacity of MO and MB onto CNTs-A is also higher than that of many other reported adsorbents.[35−45] A comparison of the adsorption capacities of MO and MB onto various adsorbents are shown in Tables 3 and 4, which suggests

Table 3. Comparison of the Adsorption Capacities of MO onto Various Adsorbents

adsorbents	adsorption capacity (mg/g)	ref
CNTs-A	149	this work
CNTs	51.7	35
hyper-cross-linked polymeric adsorbent	70	37
silkworm exuviae	87	38
chitosan/Fe_2O_3/CNTs	66	39

Table 4. Comparison of the Adsorption Capacities of MB onto Various Adsorbents

adsorbents	adsorption capacity (mg/g)	ref
CNTs-A	400	this work
CNTs	35.4−64.7	41
iron terephthalate (MOF-235)	187	36
graphene/magnetite composite	43.08	42
anaerobic granular sludge	212	44
activated Carbon	123	45

that the CNTs-A adsorbents hold great potential for dye removal from aqueous solutions. The R_L value of CNTs-A is 0.016 for MB and 0.02 for MO; the R_L value of CNTs is 0.04 for MB and 0.03 for MO, indicating that the adsorption of dyes onto CNTs and CNTs-A are favorable, and the CNTs-A is an excellent adsorbent material for dye removal from aqueous solution.

To deepen the understanding of adsorption mechanism, D-R isotherm model was chosen to describe adsorption on both homogenous and heterogeneous surfaces.[46] The D-R isotherm model was also applied to distinguish between physical and chemical adsorption of dyes on CNTs and CNTs-A. The isotherm constants, E and determination coefficients are calculated and presented in Table 2. The values of E are below 5 kJ mol^{-1} for the entire range of investigated dye concentration. The value of this parameter can give important information about adsorption mechanism. When one mole of ions is transferred, its value in the range of 1-8 kJ mol^{-1} correspond to physical adsorption;[47] the value of E is between 8 and 16 kJ mol^{-1}, when the adsorption process follows by ion-exchange, whereas its value in the range of 20−40 kJ mol^{-1} is indicative of chemisorption.[48] The mean energy of dye adsorption is below 5 kJ/mol calculated by D-R isotherm model, which suggests that physical adsorption is dominating in the adsorption process between the MO/MB dyes and adsorbents.

The thermodynamic parameters can provide in-depth information regarding the inherent energetic changes associated with the adsorption. Free energy of adsorption(ΔG^o) can be calculated from the variation of the thermodynamic equilibrium constant K_0 with the change in temperature. For adsorption reactions, K_0 is defined as follows

$$K_0 = \frac{a_s}{a_e} = \frac{v_s}{v_e}\frac{q_e}{C_e} \tag{17}$$

where a_s is the activity of adsorbed dye, a_e is the activity of dye in solution at equilibrium, q_e is the amount of dye adsorbed by per unit mass of CNTs-A(mg/g), vs is the activity coefficient of the adsorbed dye and ve is the activity coefficient of dye in solution. As dye concentration in the solution decreases and approaches zero, K_0 can be obtained by plotting ln (q_e/C_e) vs q_e and extrapolating q_e to zero, as shown in Figure 5. A linear regression analysis finds that the straight line fits the data well, and the values of K_0 are obtained from the straight line intercept with the vertical axis. The calculated values of K_0 are 10.8 for MO and 13.5 for MB at 298 K, respectively.

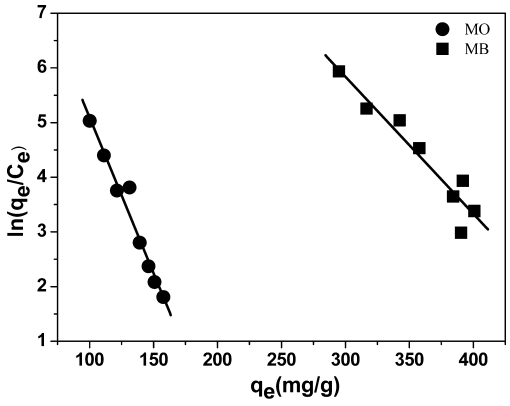

Figure 5. Plots of ln q_e/C_e vs. q_e for calculation of thermodynamic parameters.

dx.doi.org/10.1021/am301053m | ACS Appl. Mater. Interfaces 2012, 4, 5749−5760

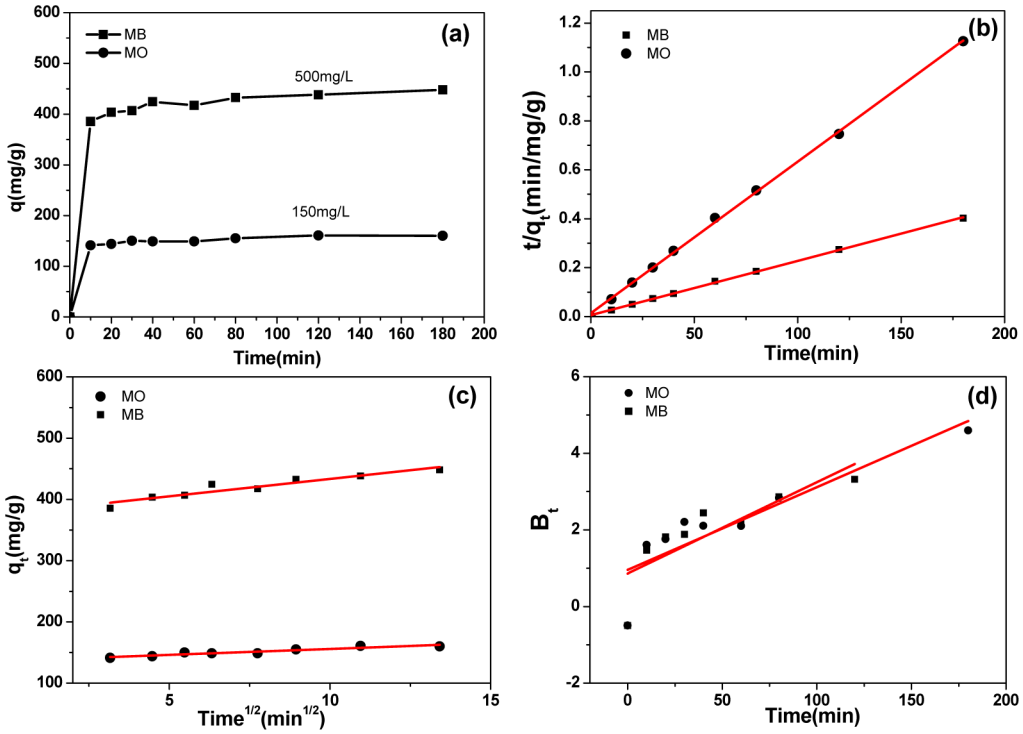

Figure 6. (a) Kinetic curves, (b) pseudo-second-order model, (c) Weber–Morris model, and (d) Boyd model of CNTs-A.

Table 5. Kinetic Parameters of Pseudo First-Order and Second-Order Adsorption Kinetic Models and Weber–Morris Model for MO and MB on CNTs-A (MO dye concentration = 150 mg/L, MB dye concentration = 500 mg/L, CNTs-A = 0.75 g/L)

			pseudo-first-order model			pseudo-second-order model			Weber–Morris model		
dye	initial conc. (mg/L)	$q_{e,exp}$ (mg/g)	k_1(min)$^{-1}$	$q_{e,cal}$ (mg/g)	R^2	k_2(min)$^{-1}$	$q_{e,cal}$ (mg/g)	R^2	K_i(g mg^{-1} min$^{-0.5}$)	C (mg/g)	R^2
MO	150	160.9	0.046	5.35	0.368	0.002	161.3	0.999	1.933	136.5	0.892
MB	500	448.1	0.070	16.3	0.730	0.0007	454.5	0.999	5.674	376.6	0.902

Free energy of adsorption(ΔG°) can be calculated to predict the process of adsorption, using the following equations

$$\Delta G^\circ = -RT\ln K_o \quad (18)$$

The ΔG° values are −5.9 kJ/mol (MO) and −6.4 kJ/mol (MB) at pH 7 and 298 K, respectively, confirming that the adsorption of MO and MB onto CNTs-A was spontaneous and thermodynamically favorable. Generally ΔG° for physisorption is less than that for chemisorption. The former is between −20 and 0 kJ/mol and the latter is between −80 and −400 kJ/mol. Therefore, the ΔG° results implied that physisorption might dominate the adsorption of MO and MB onto CNTs-A.

3.3. Adsorption Kinetics. Adsorption is a physicochemical process that involves mass transfer of a solute from liquid phase to the adsorbent surface. The transient behavior of the dye adsorption process was analyzed by using different kinetic models. Pseudo-first-order (PF) and pseudo-second-order (PS) kinetic models are adsorption reaction models, which originate from chemical reaction kinetics. To study the adsorption kinetics of MO and MB on CNTs-A, 150 mg/L (MO) and 500 mg/L (MB) initial concentrations of corresponding dye solutions were used. The adsorption removal of dyes on CNTs-A was found to be rapid at the initial period (∼15 min) and then became slow and stagnate with the increase in contact time (∼15 to ∼60 min), and nearly reached a plateau after approximately 60 min of the experiment as shown in Figure 6a. Generally the removal rate of pollutants is rapid initially, but it gradually decreases with time until it reaches equilibrium. This phenomenon is attributed to the fact that a large number of vacant adsorption sites are available for adsorption at the initial stage, and after a lapse of time, the remaining vacant adsorption sites are difficult to occupy because of repulsive forces between the solute molecules on the solid and bulk phases.[10,49] Contact time is one of the most important parameters for practical applications. It was found that the CNTs-A showed a much higher adsorption rate than that of a commercial activated carbon[50] and other adsorbents,[51] because of its desirable mesoporous structure, electrostatic attraction[34] or $\pi-\pi$ stacking interaction effect,[53] particularly for adsorption of the large molecule anionic dye with aromatic ring.

To understand the characteristics of the adsorption process, the PF and PS kinetic models were applied to fit experimental data obtained from batch experiments. The kinetic parameters and the determination coefficients (R^2) were determined by nonlinear regression and are given in Table 5. The R^2 values of the PS kinetic model are much higher than those of PF, the calculated q_e values ($q_{e,cal}$) of PS models are close to the experimental ones ($q_{e,exp}$). Hence, the PS kinetic model is more appropriate to describe the adsorption behavior of MO or MB onto CNTs-A.

If the movement of adsorbate from the bulk liquid to the liquid film surrounding the adsorbent is ignored, the adsorption process in porous solids can be separated into three stages as follows: (1) external mass transfer of adsorbate across the liquid

dx.doi.org/10.1021/am301053m | ACS Appl. Mater. Interfaces 2012, 4, 5749−5760

film to the adsorbent exterior surface, which is also called film diffusion (or boundary layer diffusion or outer diffusion); (2) transport of adsorbate from the adsorbent exterior surface to the pores or capillaries of the adsorbent internal structure, which is called intraparticle diffusion (or inner diffusion); (3) the adsorbate is adsorbed onto the active sites in inner and outer surfaces of adsorbent.[52] The third step is considered to be very fast and thus cannot be treated as rate limiting step. Generally, the adsorption rate is controlled by outer diffusion or inner diffusion or both. To determine the actual rate-controlling step involved in the MO and MB sorption process, we applied the Weber–Morris equation. Plots of q_t against $t^{1/2}$ are shown in Figure 6c, and the corresponding kinetic parameters are listed in Table 5. It was also observed that the regression of q_t versus $t^{1/2}$ was linear and the plots do not pass through the origin, suggesting that the intra-particle diffusion is not the sole rate-controlling step[53] and the external mass transfer maybe also significant in the rate-controlling step because of the large intercepts of linear portion of the plots.[54] So the overall adsorption process may be jointly controlled by external mass transfer and intraparticle diffusion, and intra-particle diffusion played a predominant role in controlling the adsorption process.

The adsorption kinetic data was further analyzed by Boyd model.[28] The calculated B_t values were plotted against time t as shown in Figure 6d. The linearity of the plots provides useful information to distinguish between external mass transfer and intraparticle diffusion controlled mechanism of adsorption.[55] The plots in Figure 6d do not pass through the origin, confirming the involvement of external mass transfer in the entire adsorption process.[5] However, the plots are not straight lines, indicating that external mass transfer shows a relatively weak rate control for dye adsorption onto CNTs-A. These results again confirm the rate-controlling mechanism of adsorption stated in Weber–Morris kinetic model studies.

3.4. Effect of Ionic Strength. Since sodium chloride is often used as a stimulator in dying processes, we tested the effect of ionic strength (NaCl) on adsorption of MO and MB onto CNTs-A, as shown in Figure 7. The increasing ionic strength in the solution causes an increase in the adsorption of MO and MB dye onto CNTs-A at pH 7, however, this increase reached a plateau at a salt concentration of 0.2 M. Ionic strength affects the activity coefficients of OH^-, H_3O^+ and specifically the adsorbable dye ions. Theoretically, when the electrostatic forces between the adsorbent surface and adsorbate ions are attractive, an increase in ionic strength will decrease the adsorption capacity. Conversely, when the electrostatic attraction is repulsive, an increase in ionic strength will increase adsorption.[56] Figure 8b shows that CNTs-A and MO were negatively charged, and MO was positively charge at pH 7 (pH_{pzc} 2 of CNTs-A). The results of MO can be explained for the electrostatic repulsion force decrease with the NaCl addition, but the experimental results of MB did not follow this convention, as the adsorption of positively charged MB dye molecules on negatively charged CNTs-A increased with the NaCl addition. The significant increase in MB removal after NaCl addition can be attributed to an increase in dimerization of MB dye in solution. The effect of NaCl on the dimerization of dye has also been investigated.[57] Various mechanisms have been suggested to explain this aggregation. These forces can be attributed to van der Waals forces, ion–dipole forces, dipole–dipole forces, and dispersion forces arising from delocalized π electrons, which occur between dye molecules in the solution. Accordingly, the higher adsorption capacity of MB under these conditions can be attributed to the aggregation of MB dye molecules induced by the action of salt ions, i.e., salt ions force dye molecules to aggregate, increasing the extent of sorption on the CNTs-A surface. Some similar study have reported an increase in dye (brilliant blue, reactive red and reactive yellow) adsorption after adding salt to the solution.[57,58]

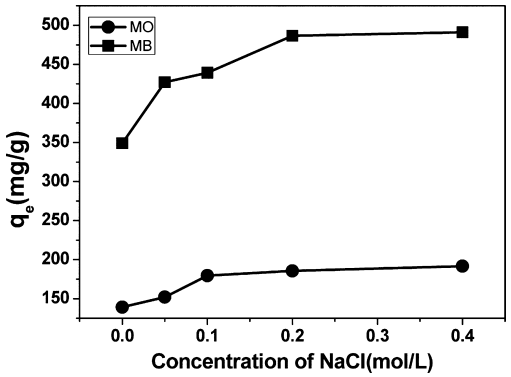

Figure 7. Effect of ionic strength on adsorption capacity of MO and MB on CNTs-A (MO concentration = 150 mg/L, MB concentration = 350 mg/L, CNTs-A = 0.75 g/L).

3.5. Effect of pH. The solution pH can affect the surface charge of the adsorbent, the degree of ionization of different pollutants, the dissociation of functional groups on the active sites of the adsorbent as well as the structure of the dye. So the influence of pH on the removal of MO and MB by CNTs-A was studied to investigate further the adsorption process. Figure 8a shows the effect of initial pH on the removal of MO and MB onto CNTs-A. The results indicate that removal of MO is less sensitive to the initial pH variation of the dye solution and remains almost a constant over the pH range of 2–10. It agrees with the previous results,[59] which showed no influence of pH on the removal of MO dyes onto CNTs-A. MO has two different chemical structures, whose chromophores are anthraquinone or azo bond depending on the pH of the solution.[60] The pH of the system exerts a profound influence on the adsorptive uptake of adsorbate molecules presumably due to its influence on the surface properties of the adsorbate molecule. After alkali-activation treatment, hydrophilic oxygen-containing functional groups, including hydroxyl, carboxylic, and carbonyl groups, were introduced into the outmost surface and defects sites of CNTs-A. The pH value for a zero charge of the CNTs-A was found to be 2. Figure 8b shows that the charge sign on the surface of CNTs-A adsorbent is negative in a wide pH range (i.e., 2–11) and the charge increases with increasing pH values. Minute change of adsorption capacity for MO, with pH variation of the dye solution suggests that the electrostatic interaction is not the primary adsorption mechanism between anionic dyes and the partially negative charged CNTs-A surface. So the adsorption of MO may not be attributed to the electrostatic interaction, therefore, other mechanisms like π–π interactions between bulk π systems on CNTs-A surfaces and organic molecules with C=C or benzene rings of MO, hydrogen bonds[61,62] can be beneficial to the adsorption. Thus a more detailed study is necessary to clearly understand the mechanism of MO adsorption on CNTs-A.

It was observed that removal of MB remains almost constant over the pH range of 4-8, and the adsorption capacity of CNTs-

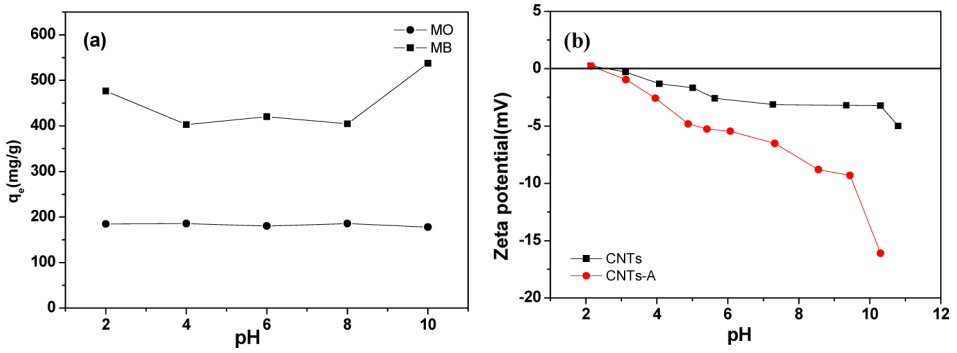

Figure 8. Adsorption capacity (a) of MO and MB on CNTs-A at different pH values (MO concentration = 150 mg/L, MB concentration = 500 mg/L, CNTs-A = 0.75g/L) and the zeta potential (b) of CNTs and CNTs-A.

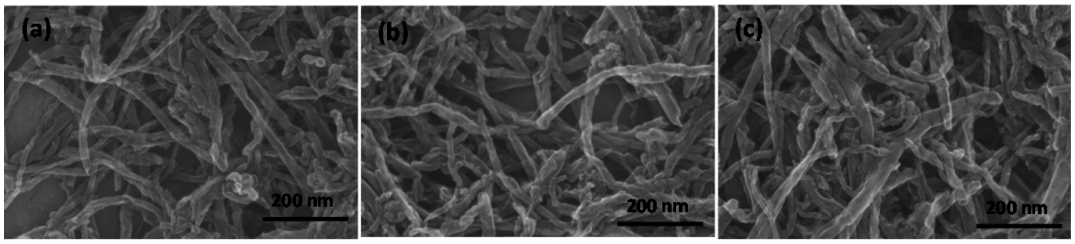

Figure 9. SEM of CNTs-A, MO adsorbed CNTs-A, MB adsorbed CNTs-A.

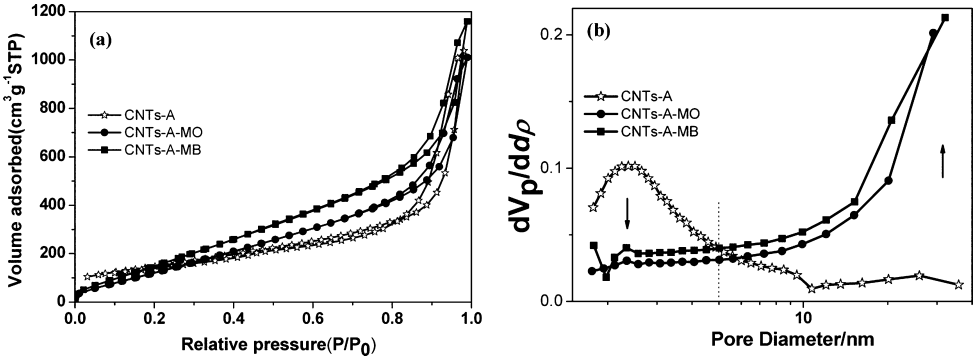

Figure 10. (a) N_2 adsorption/desorption isotherms and (b) pore size distribution of CNTs-A before and after adsorption of MO and MB.

A increased when pH <4 and pH >8, similar to previously reported results.[63] The increasing adsorption capacity of MB with the change of pH values is also due to the competition between cationic dyes and excess OH^-/H^+ ions in the solution. With the increasing of OH^- addition, more MB^+ was adsorbed on the CNTs-A by electrostatic interaction. When the pH increasing, the MB and CNTs-A are negatively charged (pHpzc 2.0 of CNTs-A), so the electrostatic interaction did not explain accurately the experimental results of MB adsorption. Therefore, other mechanism like $\pi-\pi$ electron-donor-acceptor (EDA) interaction and pore-filling[61,62] can be beneficial to the adsorption.

3.6. Adsorption Mechanism. In this study, SEM was used to assess the morphological feature and surface characteristic changes of CNTs-A before and after adsorpiton of dyes. Typical SEM photographs of CNTs-A, MO adsorbed CNTs-A and MB adsorbed CNTs-A are shown in Figure 9. The morphology of the loaded adsorbent showed some important characteristics: the surface of the CNTs-A turned to light color (Figure 9b,c) with the formation of a white layer after dye adsorption, which can be attribute to the accumulation of dye molecules over the adsorbent surface. The diameter of CNTs-A-MB was more than that of CNTs-A, as shown in Figure 9c. SEM studies visualized the formation of the molecular cloud of the dye over the surface. The above observation was further confirmed well with the batch adsorption experimental studies.

Adsorption reaction may lead to change in molecular and crystalline structures of the adsorbent and hence an understanding of the molecular structure and crystalline structures of the adsorbent and the resulting changes thereof would provide valuable information regarding adsorption reaction.[64,65] The XRD patterns taken before and after the adsorption are shown in Figure S2 in the Supporting Information, which does not show any appreciable changes in the spectra, and no other peaks corresponding to impurities were detected. The result suggests that the MO/MB dye adsorbed CNTs-A did not alter the chemical structure of adsorbent, i.e., the adsorption is physical in nature.

Q_m is the monolayer adsorption capacity (mg/g), which can be calculated by $SSA/(S_{dye}N)M_{dye}1000$,[61] where N is the Avogadro constant(6.02×10^{23}), M_{dye} is the molecular weight (g/mol), and S_{dye} is the projecting area of a single adsorbate molecule (m^2). And the the Q_m of MO and MB is 1037 and 516 mg/g, respectively, which are higher than the computed

dx.doi.org/10.1021/am301053m | ACS Appl. Mater. Interfaces 2012, 4, 5749−5760

maximum monolayer capacities(149 mg/g for MO and 400 mg/g for MB). The results indicate that MO and MB were adsorbed on the heterogeneous adsorption surface of CNTs-A with sites having different adsorption energies and not equally available according to the Freundlich model fitting results. When the pore diameter is below 5 nm, the mesopore volume of dye adsorbed CNTs-A decreased after adsorption, as shown in Figure 10 and Table 1, which can be explained as that mesopores may favor the adsorbate-adsorbate interaction via mesopore filling mechanism. However, the mesopore volume increased dramatically when the pore diameter is larger than 5 nm, which indicates that large quantities of new pores have been produced after adsorption. Dye ions have a tendency to self-associate (or aggregate) in aqueous solution.[66,67] At low dye concentrations, dyes form dimers with dimerization essentially complete before further aggregation occurs. Subsequent aggregation will take place initially between dimeric units.[68] Hence, the adsorption space may accommodate more than one layer of molecules and not all adsorbed molecules are in contact with the surface layer of the adsorbent. So the SSA and PV may be increased after adsorption for multilayer adsorption and aggregation of dyes on the surface of CNTs-A, as schematically illustrated in Figure 11.

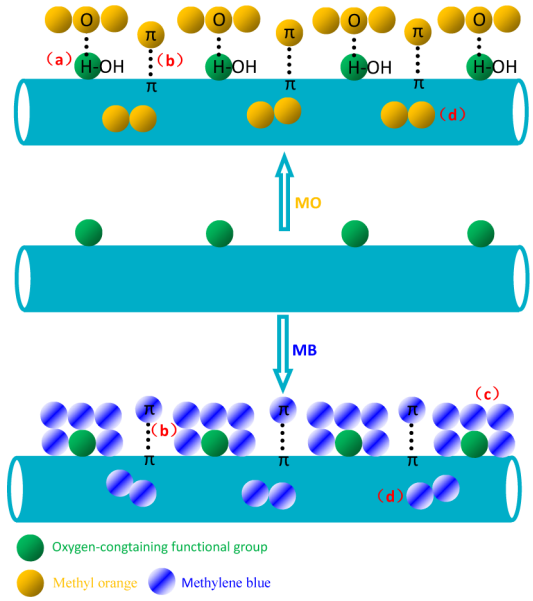

Figure 11. Adsorption schematic diagrams of MO or MB on CNTs-A though (a) hydrogen bonding, (b) $\pi-\pi$ EDA interactions, (c) electrostatic interactions, (d) mesopore filling.

FTIR spectra analysis was performed to gain insights into the adsorption mechanism. FTIR spectra analyses of CNTs-A, MO/MB dyes, and MO/MB adsorbed CNTs-A are shown in Figure 12. FTIR study of CNTs-A confirms the defective sites at the surface of CNTs-A and the presence of −OH (3409 cm^{-1}), >C═C (1686 cm^{-1}), −C═O (1548 cm^{-1}) and >C−O (1066 cm^{-1}) functional groups at the surface of CNTs-A, which leads to the hydrophilic nature of CNTs-A. These functional groups may also act as anchoring sites for dye molecules. In the case of MO, peaks at 1013, 1185, and 1,355 cm^{-1} correspond to −S═O, CH_3−, C−N of MO dyes, respectively, whereas the peak at 1590 cm^{-1} corresponds to N═N group. FTIR spectra of MO adsorbed CNTs-A show new peaks at 798 and 895 cm^{-1}, which are all located in the finger print region. The

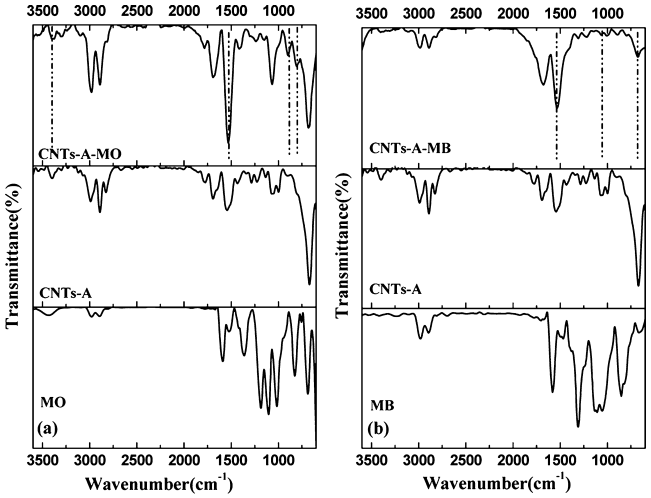

Figure 12. FTIR spectra of pure MO or MB, and CNTs-A before and after adsorption of (a) MO or (b) MB.

intensities of peaks at 1548 and 1687 cm^{-1} increased due to −N═N− group attached to the aromatic ring of MO dyes, which indicates that MO has been anchored on the surface of CNTs-A during the adsorption. After the MO adsorption, the intensity of peak at 3409 cm^{-1} increased, which indicates that hydrogen bonding interaction may be an important process for MO adsorption onto CNTs-A. After KOH-activation treatment, more oxygen-containing functional group have been modifed on the surface of CNTs-A, and the hydrophilic properties of CNTs-A have been improved. More importantly, the oxygen atom of the S═O group can be used as the hydrogen-bonding acceptor and from intramolecular hydrogen bonding with the hydrogen atom of the hydroxyl group of CNTs-A, as schematically illustrated in Figure 11a. In the case of MB, peaks at 1088, 1312 and 1590 cm^{-1} correspond to CH_3−, C−N, C═S, respectively, as shown in Figure 10b. After adsorption of MB, a shift in the 1522 cm^{-1} peak (now at 1540 cm^{-1}) was observed, and the peak sharpen and showed a significant increase in intensity which may correspond to the attachment of MB on the surface of CNTs-A (Figure 10b). It should be noted that the peaks associated with the V_{C-O} (1066 cm^{-1}) and $V_{=CH}$ (681 cm^{-1}) for the CNTs-A seem to be broadened and showed a significant decrease in intensity. MB is a type of cationic dye which can be adsorbed easily by electrostatic forces on negatively charged surfaces, as schematically illustrated in Figure 11c. Therefore, the change in V_{C-O} after adsorption may be ascribed to the electrostatic attraction between CNTs-A and MB. The increase of adsorbed MB with increasing pH is shown in Figure 8a. Similar to previously reported results, this result might be due to the fact that the concentration of negative charges of the adsorbent increases with increasing pH. As we all known that MB is also an ideal planar molecule; therefore, a mechanism of $\pi-\pi$ EDA interaction between MB (π-electron-acceptors) and the π electron-rich regions on the graphene surface of CNTs-A is plausible, which may lead to the weakening intensity of $V_{=CH}$ for CNTs-A. The FTIR spectra analysis indicated that MB might be easily adsorbed through CNTs-A by $\pi-\pi$ stacking interactions and electrostatic attractions, as schematically illustrated in Figure 11

4. CONCLUSION

We have developed an alkali-activation method for the synthesis of activated CNTs (CNTs-A) with higher SSA and PV. The resulting CNTs-A were demonstrated as an efficient adsorbent material for removal of anionic and cationic dyes in aqueous solutions. As suggested by our experimental data, CNTs-A showed excellent adsorption capacity of 149 mg/g for MO and 400 mg/g for MB, which can be attributed to multiple adsorption interaction mechanisms (e.g., hydrogen bonding, $\pi-\pi$ EDA interactions, electrostatic interactions, mesopore-filling) between dyes and adsorbent. This finding indicates that alkali-activation is a useful method to improve the adsorption affinity of dye contaminants on CNTs-A. Therefore, the activated CNTs may be a promising adsorbent nanomaterial for organic pollutants in aqueous solutions.

■ ASSOCIATED CONTENT

Supporting Information

Maximum adsorption capacity of MO/MB, XRD pattern of CNTs-A before and after adsorption, characteristics and structures of MB/MO. This material is available free of charge via the Internet at http://pubs.acs.org.

■ AUTHOR INFORMATION

Corresponding Author

*E-mail: jhchen@uwm.edu (J.H.C.); fyu@vip.163.com (F. Y.).

Notes

The authors declare no competing financial interest.

■ ACKNOWLEDGMENTS

This research was supported by the National Natural Science Foundation of China (21207100, 21177095), State Key Laboratory of Pollution Control and Resource Reuse Foundation (PCRRY11009), Scholarship Award for Excellent Doctoral Student granted by Ministry of Education. We are also thankful to anonymous reviewers for their valuable comments to improve this manuscript.

■ REFERENCES

(1) El Boujaady, H.; El Rhilassi, A.; Bennani-Ziatni, M.; El Hamri, R.; Taitai, A.; Lacout, J. L. *Desalination* **2011**, *275*, 10−16.
(2) Gupta, V. K.; Mittal, A.; Malviya, A.; Mittal, J. *J Colloid Interface Sci.* **2009**, *335*, 24−33.
(3) Gupta, V. K.; Gupta, B.; Rastogi, A.; Agarwal, S.; Nayak, A. *J. Hazard. Mater.* **2011**, *186*, 891−901.
(4) Gupta, V. K.; Ali, I. *Environ. Sci. Technol.* **2008**, *42*, 766−770.
(5) Gupta, V. K.; Mittal, A.; Gajbe, V.; Mittal, J. *J. Colloid Interface Sci.* **2008**, *319*, 30−39.
(6) Yang, O. B.; Lee, H. C.; Akhtar, M. S.; Park, J. G.; Kim, K. J.; Lee, S. K. *J. Nanosci. Nanotechnol.* **2010**, *10*, 3502−3507.
(7) Hu, J.; Shao, D. D.; Chen, C. L.; Sheng, G. D.; Li, J. X.; Wang, X. K.; Nagatsu, M. *J. Phys. Chem. B* **2010**, *114*, 6779−6785.
(8) Hyung, H.; Kim, J. H. *Environ. Sci. Technol.* **2008**, *42*, 4416−4421.
(9) Chen, W.; Duan, L.; Zhu, D. Q. *Environ. Sci. Technol.* **2007**, *41*, 8295−8300.
(10) Ghaedi, M.; Hassanzadeh, A.; Kokhdan, S. N. *J. Chem. Eng. Data* **2011**, *56*, 2511−2520.
(11) Ghaedi, M.; Sadeghian, B.; Pebdani, A. A.; Sahraei, R.; Daneshfar, A.; Duran, C. *Chem. Eng. J.* **2012**, *187*, 133−141.
(12) Ghaedi, M.; Biyareh, M. N.; Kokhdan, S. N.; Shamsaldini, S.; Sahraei, R.; Daneshfar, A.; Shahriyar, S. *Mater. Sci. Eng., C* **2012**, *32*, 725−734.
(13) Ghaedi, M.; Shokrollahi, A.; Tavallali, H.; Shojaiepoor, F.; Keshavarz, B.; Hossainian, H.; Soylak, M.; Purkait, M. K. *Toxicol. Environ. Chem.* **2011**, *93*, 438−449.
(14) Fletcher, A. J.; Yuzak, Y.; Thomas, K. M. *Carbon* **2006**, *44*, 989−1004.
(15) Kang, H. Y.; Park, S. S.; Rim, Y. S. *Kor. J. Chem. Eng.* **2006**, *23*, 948−953.
(16) Hameed, B. H.; Foo, K. Y. *Desalination* **2011**, *275*, 302−305.
(17) Huang, C. C.; Chen, C. H. *Int. J. Hydrogen Energy* **2007**, *32*, 237−246.
(18) Song, S. Q.; He, C. X.; Liu, J. C.; Maragou, V.; Tsiakaras, P. *J. Power Sources* **2010**, *195*, 7409−7414.
(19) Ma, J.; Wang, J. N.; Wang, X. X. *J. Mater. Chem.* **2009**, *19*, 3033−3041.
(20) Ma, J.; Wang, J. N. *Chem. Mater.* **2008**, *20*, 2895−2902.
(21) Behnajady, M. A.; Modirshahla, N.; Fathi, H. *J. Hazard. Mater.* **2006**, *136*, 816−821.
(22) Davranche, M.; Lacour, S.; Bordas, F.; Bollinger, J. C. *J. Chem. Educ.* **2003**, *80*, 76−78.
(23) Menendez, J. A.; Illangomez, M. J.; Leon, C. A. L. Y.; Radovic, L. R. *Carbon* **1995**, *33*, 1655−1657.
(24) Sonawane, G. H.; Shrivastava, V. S. *Desalin. Water Treat.* **2011**, *29*, 29−38.
(25) Ho, Y. S.; McKay, G. *Chem. Eng. J.* **1998**, *70*, 115−124.
(26) Hobson, J. P. *J. Phys. Chem.* **1969**, *73*, 2720−2727.
(27) Weber, W. J.; Morris, J. C. *J. Sanitary Eng. Div.* **1963**, *89*, 31−60.
(28) Kumar, K. V.; Ramamurthi, V.; Sivanesan, S. *J. Colloid Interface Sci.* **2005**, *284*, 14−21.
(29) Lillo-Rodenas, M. A.; Cazorla-Amoros, D.; Linares-Solano, A. *Carbon* **2003**, *41*, 267−275.
(30) Lillo-Rodenas, M. A.; Juan-Juan, J.; Cazorla-Amoros, D.; Linares-Solano, A. *Carbon* **2004**, *42*, 1371−1375.
(31) Langmuir, I. *J. Am. Chem. Soc.* **1918**, *40*, 1361−1403.
(32) Freundlich, H. M. F. *J. Phys. Chem.* **1906**, *57*, 385−471.
(33) Yu, F.; Ma, J.; Wu, Y. Q. *J. Hazard. Mater.* **2011**, *192*, 1370−1379.
(34) Ai, L. H.; Zhang, C. Y.; Liao, F.; Wang, Y.; Li, M.; Meng, L. Y.; Jiang, J. *J. Hazard. Mater.* **2011**, *198*, 282−290.
(35) Yao, Y. J.; He, B.; Xu, F. F.; Chen, X. F. *Chem. Eng. J.* **2011**, *170*, 82−89.
(36) Haque, E.; Jun, J. W.; Jhung, S. H. *J. Hazard. Mater.* **2011**, *185*, 507−511.
(37) Huang, J. H.; Huang, K. L.; Liu, S. Q.; Wang, A. T.; Yan, C. *Colloids Surf., A* **2008**, *330*, 55−61.
(38) Chen, H.; Zhao, J.; Wu, J. Y.; Dai, G. L. *J. Hazard. Mater.* **2011**, *192*, 246−254.
(39) Zhu, H. Y.; Jiang, R.; Xiao, L.; Zeng, G. M. *Bioresour. Technol.* **2010**, *101*, 5063−5069.
(40) Chen, S. H.; Zhang, J.; Zhang, C. L.; Yue, Q. Y.; Li, Y.; Li, C. *Desalination* **2010**, *252*, 149−156.
(41) Yao, Y. J.; Xu, F. F.; Chen, M.; Xu, Z. X.; Zhu, Z. W. *Bioresour. Technol.* **2010**, *101*, 3040−3046.
(42) Ai, L. H.; Zhang, C. Y.; Chen, Z. L. *J. Hazard. Mater.* **2011**, *192*, 1515−1524.
(43) Xie, H. J.; Tan, W.; Zhang, J. A.; Niu, H. B. *Adv Mater Res-Switz* **2011**, *152-153*, 691−696.
(44) Liu, F. F.; Teng, S. X.; Song, R. H.; Wang, S. G. *Desalination* **2010**, *263*, 11−17.
(45) Suresh, S.; Sugumar, R. W.; Maiyalagan, T. *Asian J. Chem.* **2011**, *23*, 4486−4490.
(46) Jovanovic, B. M.; Vukasinovic-Pesic, V. L.; Rajakovic, L. V. *Water Environ. Res.* **2011**, *83*, 498−506.
(47) Onyango, M. S.; Kojima, Y.; Aoyi, O.; Bernardo, E. C.; Matsuda, H. *J. Colloid Interface Sci.* **2004**, *279*, 341−350.
(48) Tahir, S. S.; Rauf, N. *Chemosphere* **2006**, *63*, 1842−1848.
(49) Apul, O. G.; Shao, T.; Zhang, S. J.; Karanfil, T. *Environ. Toxicol. Chem.* **2012**, *31*, 73−78.
(50) Iriarte-Velasco, U.; Chimeno-Alanis, N.; Gonzalez-Marcos, M. P.; Alvarez-Uriarte, J. I. *J Chem Eng Data* **2011**, *56*, 2100−2109.

(51) Crini, G. *Bioresour. Technol.* **2006**, *97*, 1061−1085.
(52) Rengaraj, S.; Kim, Y.; Joo, C. K.; Yi, J. *J. Colloid Interface Sci.* **2004**, *273*, 14−21.
(53) Dogan, M.; Abak, H.; Alkan, M. *J. Hazard. Mater.* **2009**, *164*, 172−181.
(54) Al-Degs, Y. S.; El-Barghouthi, M. I.; Issa, A. A.; Khraisheh, M. A.; Walker, G. M. *Water Res.* **2006**, *40*, 2645−2658.
(55) Sankar, M.; Sekaran, G.; Sadulla, S.; Ramasami, T. *J. Chem. Technol. Biotechnol.* **1999**, *74*, 337−344.
(56) Alberghina, G.; Bianchini, R.; Fichera, M.; Fisichella, S. *Dyes Pigm.* **2000**, *46*, 129−137.
(57) Al-Degs, Y. S.; El-Barghouthi, M. I.; El-Sheikh, A. H.; Walker, G. A. *Dyes Pigm.* **2008**, *77*, 16−23.
(58) German-Heins, J.; Flury, M. *Geoderma* **2000**, *97*, 87−101.
(59) Aravindhan, R.; Fathima, N. N.; Rao, J. R.; Nair, B. U. *Colloids Surf., A* **2007**, *299*, 232−238.
(60) Yu, F.; Chen, J. H.; Chen, L.; Huai, J.; Gong, W. Y.; Yuan, Z. W.; Wang, J. H.; Ma, J. *J. Colloid Interface Sci.* **2012**, *378*, 175−183.
(61) Lin, D. H.; Xing, B. S. *Environ. Sci. Techno.l* **2008**, *42*, 7254−7259.
(62) Pan, B.; Xing, B. S. *Environ. Sci. Technol.* **2008**, *42*, 9005−9013.
(63) Rafatullah, M.; Sulaiman, O.; Hashim, R.; Ahmad, A. *J. Hazard. Mater.* **2010**, *177*, 70−80.
(64) Namasivayam, C.; Kavitha, D. *Microchem J* **2006**, *82*, 43−48.
(65) Ikhtiyarova, G. A.; Ozcan, A. S.; Gok, O.; Ozcan, A. *Clay Miner.* **2012**, *47*, 31−44.
(66) Hamada, K.; Yamada, K.; Mitsuishi, M.; Ohira, M.; Mesuda, K. *J. Chem. Soc., Faraday Trans.* **1995**, *91*, 1601−1605.
(67) Nizamov, S. N.; Barakaeva, M. N.; Kurtaliev, E. N.; Tatarets, A. L.; Patsenker, L. D. *J. Appl. Spectrosc.* **2009**, *76*, 464−469.
(68) Walker, G. M.; Weatherley, L. R. *Chem. Eng. J.* **2001**, *83*, 201−206.